Advanced UAV
http://publish.mersin.edu.tr/index.php/uav
e-ISSN 2822-6976

Analysis of pneumatic catapult launch system parameters, taking into account engine and UAV characteristics

Alexander Khrulev[*1]

[1]*Kharkiv National Automobile and Highway University, Automobile Department, Ukraine, info@engine-expert.com*

Cite this study: Khrulev, A. (2023). Analysis of pneumatic catapult launch system parameters, taking into account engine and UAV characteristics. Advanced UAV, 3 (1), 10-24

Keywords
UAV
Launch system
Pneumatic
Catapult

Research Article
Received:27.04.2023
Revised: 15.05.2023
Accepted:27.05.2023
Published:01.06.2023

Abstract

Despite progress in the development of unmanned aerial vehicles (UAVs), universal launch systems are not currently used for them. In fact, each UAV project requires its own launcher, which is inefficient in many cases, especially for heavy UAVs weighing 50 kg or more, for which pneumatic launch systems are mainly used. To evaluate the characteristics of UAV launchers, simple methods are used at the level of analysis of acting forces, but they do not make it possible to correctly select the type and parameters of the catapult for specific tasks. In the absence of the necessary methods, this leads to design errors that significantly narrow the scope of the launcher. To eliminate these problems, a mathematical model of a pneumatic catapult has been developed, differential equations of motion and changes in the gas-dynamic parameters of structural elements have been compiled and numerically solved, an analysis of the structural scheme and basic parameters of the pneumatic launch system has been performed. It is shown by simulation that no special pneumatic cylinder piston sealing is required for the launcher's effective functioning, because at high air pressures leakage through the gap is controlled due to the short process time. Also, the permissible minimum height of the cable attachment point on the trolley above the block roller has been determined. The developed model confirmed the versatility of using the pneumatic launcher of the scheme under consideration for the UAVs with a take-off weight of 50 to 250 kg, and such a wide range is provided only by regulating the receiver air pressure and is not available for other types of systems. At the same time, the possibility of further increasing the takeoff weight of the UAV in the launch scheme under consideration will remain by increasing the diameter of the pneumatic cylinder.

1. Introduction

The creation of aviation unmanned systems includes the development of not only the unmanned aerial vehicle (UAV) itself and its systems, but also its launch system. Depending on the mass, purpose, and design scheme of UAVs, the launch systems show a significant variety both in types and in application features [1, 2].

If for tactical UAVs of the Micro (up to 2 kg) and Mini (2-15 kg) classes, a start from the operator or assistant hand is often used [3], then for heavy UAVs of an operational and especially strategic class, it is not uncommon to start from the concrete runway of existing airfields [4]. However, for tactical and operational-tactical UAVs in the mass range of 15 kg or more, these methods may not be effective. For example, with a mass of more than 10-15 kg, it becomes practically impossible both to launch from the operator's hand due to physical limitations and/or safety requirements. It is the same with launching from the ground due to the lack of not only an airfield, but even, possibly, a suitable hard surface area near the base. In addition, there is a limitation due to the use of fixed-pitch propellers – they cannot be designed for the best take-off performance, so as not to degrade the tactical

performance of the vehicle [5]. In addition, takeoff from the runway requires the presence of landing gear and an additional supply of fuel. This, other things being equal, increases the mass and reduces the payload of the UAV. It is the complex of such reasons that explains the fact that in the considered range of masses of vehicles, a special launch complex often has no practical alternative.

However, if the necessity to develop and use a launch complex for operational and tactical UAVs is more or less clear, then there are a large number of options for choosing the type of launch system. In addition, not all launch system working processes have been worked out in such detail that it would be easy to choose their optimal parameters for a specific task.

2. Literature review and problem statement

To date, all developed launchers for unmanned aerial vehicles can be divided into several main types, including automotive, bungee, spring, kinetic, electro-magnetic, hydraulic, pneumatic and rocket systems.

The experience of use, accumulated over many decades, makes it possible to identify the advantages and disadvantages of each type, depending on how the systems under consideration meet the basic technical requirements for UAV launch systems. The list of such requirements includes [2]:

1) starting speed range (usually 20-40 m/s);
2) range of launch angles (usually 5-200);
3) allowable takeoff weight of the UAV;
4) acceleration at launch (usually 5-10g);
5) remote launch control;
6) operating temperature range (usually from -25 to +400C;
7) weight and maximum installation length;
8) the cost of the system;
9) preparation time of the transport state, the possibility of quick disassembly for transportation and storage (usually up to 15 minutes);
10) the number of service personnel;
11) overall safety, reliability and ease of operation.

Although these requirements are taken into account in the conceptual design of catapult launch systems, other general provisions can be distinguished. So, to date, the main technical problem associated with launchers for UAVs is the accumulation of potential launch energy [5]. Depending on the type of system, there are several energy storage solutions: capacitors and batteries in electromagnetic launchers, receivers and hydraulic accumulators in pneumatic and hydraulic launch systems, elastic parts in bungee and spring launchers, solid propellant in rocket boosters, etc. That is, a common feature for all these solutions is the supply of energy in its potential form.

In addition, the design of most launchers [6] requires the use of a special trolley, on which the vehicle is installed at the start stage. The design and parameters of the launcher are largely determined by the way the launch potential energy is converted into the kinetic energy of the UAV. This can be either the action of an actuator (an elastic element, a piston, a rocket engine) directly on the booster trolley with the vehicle, or through a block or a system of blocks. After the start of the UAV, it is necessary to initiate a controlled process of braking the trolley, which also presents difficulties for some types of systems [7].

Automobile launchers [4] are the simplest and include only a special UAV mount, which ensures its disengagement after the vehicle accelerates to a given takeoff speed. The advantage of this design of the starting system is simplicity and low cost, since all the energy is provided by the car. However, an obvious disadvantage that hinders use is not only the car itself, but also the need for a large open space with a hard surface, which is difficult or impossible to provide in real conditions for a number of tasks.

UAVs weighing up to 5 kg (sometimes more) are often launched using the so-called bungee mechanisms, where the elastic bungee cord is pre-twisted with a winch or mechanically tensioned [1, 8]. Potential energy is stored in the elastic cord itself and then transferred to the mechanism holding the UAV. Such systems are relatively simple and cheap compared to others. Their design usually consists of a power frame and a set of rubber bands that act as a drive. In addition, instead of a cord, a spring can be used as an elastic element [9]. However, with an increase in the mass of the vehicle, limited efforts and other disadvantages of this type of device begin to appear, including limitations on the control of parameters and relatively rapid wear of the elastic elements.

Electrically driven devices, including synchronous magnetic launchers, were also considered, including for relatively heavy UAVs weighing several hundred kilograms [7]. However, they have not gained popularity due to the complexity of energy conversion and the need to use special brake mechanisms for the trolley after the launch of the UAV [10]. This also applies to other starting systems, such as hydraulic ones, which use compressed gas as a power source. In such systems, the oil cavity of the accumulator is connected to the starting cylinder, and

the piston in it is connected to the movable traverse of the chain hoist mechanism used to animate the movement of the trolley with the UAV with a small movement of the piston.

Inertial launch systems using the energy of a rotating flywheel did not receive a noticeable expansion within the considered range of UAV masses due to the difficulty of transferring energy to the trolley [5]. Launch systems with rocket boosters, which were previously used mainly for full-size heavy strategic-class UAVs, also turned out to be limitedly applicable.

On the contrary, pneumatic launch systems (Figure 1), where compressed air is used as a working medium, are currently the most widely used. The large energy stored during air compression makes it easy to launch UAVs weighing 50–200 kg or more [7]. These systems are relatively simple, reliable, and easily adjustable for changes in mass and takeoff speed. Compared to some other systems, such as bungee mechanisms, the cost of a pneumatic launch system may be higher, but this difference is not critical.

Figure 1. Pneumatic launcher for UAV with take-off weight 100 kg and more

The main disadvantage of the pneumatic launcher is considered to be significant overall dimensions, which can create problems during transportation. In addition, large inertia forces in the system prevent the provision of the specified parameters of the trolley movement at the stages of starting and braking [2]. However, due to many advantages, pneumatic systems currently make up the majority among other launchers [7].

In practice, 3 main structural schemes of pneumatic catapults are used (Figure 2) – direct action (1), with pulley (2) and with pulley block mechanism (3).

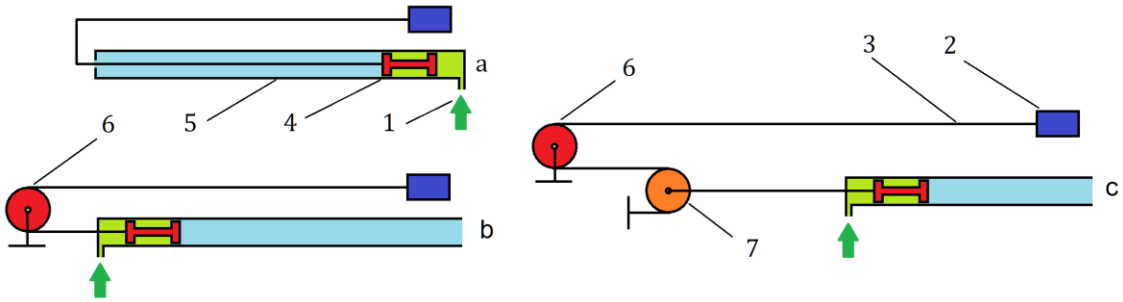

Figure 2. The main types of pneumatic catapults: a – direct action, b – with pulley, c – with pulley block mechanism, 1 – compressed air inlet, 2 – trolley with payload, 3 – cable, 4 – piston, 5 – cylinder, 6 – fixed block roller, 7 – movable roller

Direct action catapults (1) have a limited scope in terms of UAV weight (usually no more than 40–50 kg) and launch speed (less than 20 m/s) due to problems associated with large strokes of the pneumatic cylinder rod [11,12]. In addition, such systems require a special additional cylinder for braking the trolley after UAV take-off, which greatly complicates the design [7].

For the catapults, which are more complex cinematic, with a pulley block mechanism (3) and a shortened piston stroke in the cylinder, the loads on the rollers and supports increase sharply, which introduces restrictions on the mass and launch speed [9]. As a result, a simple scheme with pulley (2) may turn out to be the most effective in the widest range of UAV parameters.

However, despite the fact that a large number of works are traditionally devoted to pneumatic catapults for launching UAVs, due attention is not paid to the detailed study of the process of launching UAVs. Thus, there are a large number of review works [1,8], while theoretical research, and even more so, modeling of the system operation is often replaced by a simple analysis of acting forces [2,6]. After that, as can be understood from the examples [1,6], they immediately proceed to the launcher design, which entails the risk of choosing non-optimal parameters or even the entire design scheme [13].

Only in a small number of sources is there a more or less detailed mathematical description of the processes under consideration [14]. However, as a rule, it is limited by the chosen catapult scheme, not applicable to other kinds of launchers, and in some cases, it may even contain errors [11]. As a result, there is a rather simplified approach to the choice of launcher parameters. Perhaps this is due to the fact that in any unmanned complex the UAV is the basis, and auxiliary systems are considered according to some residual principle, since they do not directly affect the performance of the task [15,16]. This can lead not only to the choice of non-optimal parameters of the launcher and restrictions on the scope of its application, but also to the complication and rise in the cost of the entire unmanned complex due to an inefficient launch system.

In accordance with this, the purpose of the study is to develop a mathematical model, modeling and analysis of the characteristics of a pneumatic catapult when the initial parameters change over a wide range. To achieve this purpose, differential equations were compiled and numerically solved that describe the movements and thermodynamic processes of structural elements for various combinations of parameter values.

3. Material and Method

For further research, a simple scheme with a pulley was chosen (Figure 3). The choice is due to the main advantage of this scheme – the absence of a special brake mechanism for the trolley.

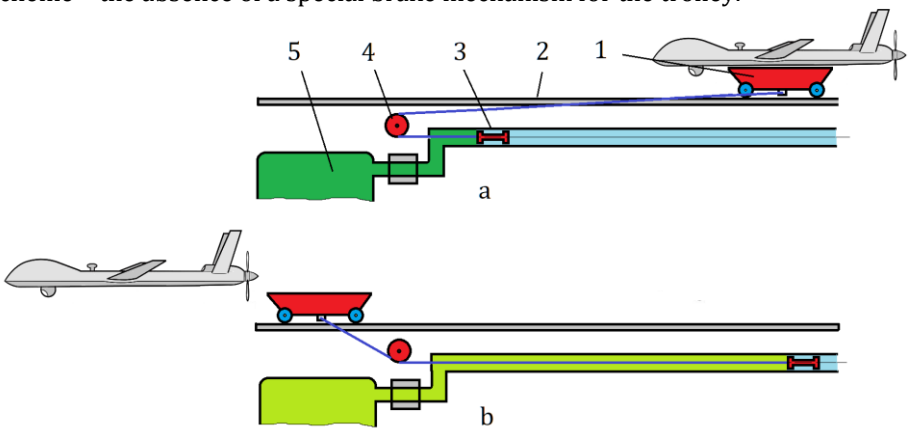

Figure 3. During the operation of the catapult with the pulley, 2 phases can be distinguished, including the acceleration phase of the trolley with the UAV (a) and the UAV start phase with the braking of the trolley (b): 1 – trolley, 2 – guides, 3 – pneumatic cylinder, 4 – pulley, 5 – receiver

As a result, the design of the launcher is extremely simple (Figure 4) – two guides with a pneumatic cylinder, connected by frames, form a power frame, a trolley on guides through a pulley is fitted to a piston by a cable, a cavity of pneumatic cylinder is connected to a receiver.

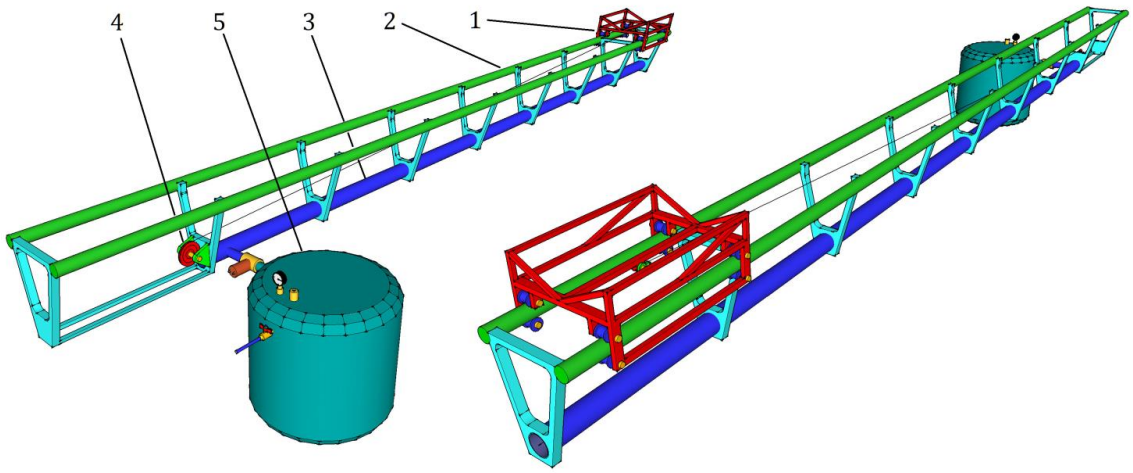

Figure 4. Structural scheme of the catapult with the inclusion of a pneumatic cylinder in the structure of the power frame (designations according to Figure 2)

Based on the obvious ratio of the masses of the trolley and the UAV, the braking of the trolley after the start should occur by pulling the piston to the side against the acceleration movement. In this case, the braking distance is assumed to be many times shorter than the acceleration length in accordance with the ratio of the masses of the UAV and the trolley, but this requires verification.

3.1. Mathematical model

At the preliminary stage of the study, the main provisions of the proposed model were formulated and a calculation algorithm was compiled. The main node of the launching system under study is the pulley (Figure 5), the vertical tangent to which determines the zero position of the trolley (x coordinate).

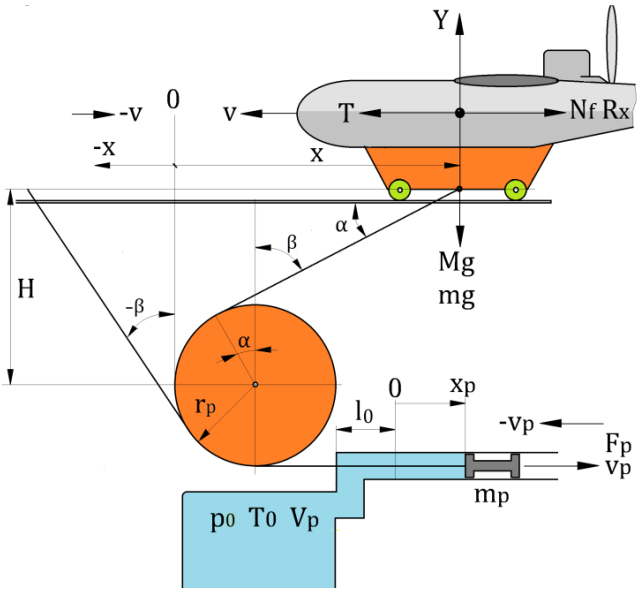

Figure 5. Calculation scheme of the pulley and acting forces: the movement of the trolley at a negative angle β leads to its automatic braking due to piston reversal

Since the piston is connected to the trolley by a cable, its movement depends on the movement of the trolley, but is not equal to it due to the presence of a variable angle of inclination of the cable α from the guides of the trolley.

In order to determine the required dependencies, it is necessary to consider the calculation scheme of the catapult in more detail.

3.1.1. Kinematics of pulley with cable

Due to the height of the guides above the pulley, the cable attachment point on the trolley is located at a height H from the pulley axis (Figure 5), and the cable pulls the trolley at an angle. Let's find the angles of the cable. Obviously:

$$H = \frac{x-r}{\tan\beta} + \frac{r}{\sin\beta}, \tag{1}$$

where $r = d/2$ is the radius of the pulley, β is the angle of the cable from the vertical, x is the coordinate of the cable attachment on the trolley from the zero position (Figure 4). In this case, the values of x are positive to the left, negative to the right, and the initial position of the trolley is at a given distance L_0 from zero.

Let's transform the Equation (1):

$$tg\beta = \frac{x-r}{H} + \frac{r}{H\cos\beta}. \tag{2}$$

Equation (2) can be converted to a square one with respect to $\cos\beta$ or $\sin\beta$, but the solution is not only cumbersome, but also ambiguous, and when passing through zero, it also changes sign. At this condition the equation can be solved by the method of successive approximations. However, in order not to complicate the task, an approximate solution was found. In Equation (2), the second term is less than the first one so $\cos\beta$ can simply be replaced by an approximate formula:

$$\cos\beta = \frac{H}{\sqrt{H^2+x^2}},$$

whence the Equation (2) gives:

$$\tan\beta = \frac{1}{H}\left[x + r\left(\sqrt{1+\left(\frac{x}{H}\right)^2} - 1\right)\right]. \quad (3)$$

For x = 0, it follows from (3) that β = 0, which exactly corresponds to the real picture (Figure 5). For large x (when β is close to 90^0), the error in the calculation by Equation (3) is small and does not exceed 20'-30', which is also quite acceptable for practical results (it means the cable pulls the trolley almost horizontally, and the displacement of the trolley and the piston are almost the same).

An important condition for the correct operation of the model is the connection of the trolley with the piston through the pulley. If we assume that the cable is absolutely rigid, then its length is constant and equal to:

$$L_c = l_1 + l_2 + l_3 + l_4, \quad (4)$$

where:

$l_1 = (H - r\ \sin\beta)/\sin\alpha$ is the length of the upper part of the cable, for which the angle is calculated by formula (3) at $x = L_0$, and $\alpha = 90^0 - \beta$ (fig. 4);

$l_2 = \pi r(90^0 + \beta)/180$ is the length of the cable part on the pulley at $x = L_0$;

$l_3 = r$ is approximate distance from the lower edge of the pulley to the end (cover) of the pneumatic cylinder;

$l_4 = l_0$ is the initial position of the piston in the cylinder from its front end;

$\alpha = 90^0 - \beta$ is the angle of inclination of the cable upper part.

When the trolley moves, the x coordinate of the cable end decreases, then the coordinate (displacement) of the piston in the cylinder x_p can be found from the condition of the cable length being constant according to the formula:

$$x_p = L_c - \frac{H - r\ \sin\beta}{\sin\alpha} - \frac{\pi r(90^0+\beta)}{180} - l_0 - r\,. \quad (5)$$

At the same time, the velocities of the trolley v and the piston v_p are also related (Figure 4):

$$v_p = v\sin\beta.$$

The choice of the formula for calculating the length of the upper part of the cable through the height H and the angle β (2) is associated with the transition of the trolley through the zero position, at which the angle β passes through 0. If the length of the cable is directly related to the trolley coordinate x, and not to the angle β, this can cause an unwanted singular point to appear in the calculation.

3.1.2. Forces acting on the launcher

The diagram of the action of forces on the trolley is shown in Figure 5. For the trolley, the equation of Newton's 2nd law is valid:

$$m_0\frac{d\vec{v}}{d\tau} = \sum_{k=0}^{n}\vec{F}_i, \quad (6)$$

It determines the acceleration $d\vec{v}/d\tau$ of a body with mass m_0 under the action of applied forces $\vec{F}_i$.

If we connect the x-axis with the guides of the catapult, then from Equation (6) we obtain an equation describing the movement of the trolley from the starting point in the form:

$$M_\Sigma\frac{dv}{d\tau} = F_{px} + T - R_x - F_f - F_{gx}, \quad (7)$$

where $M_\Sigma = M + m$ is the total mass of the accelerated system, M is the mass of the UAV, m is the mass of the trolley and the mass of the cable associated with it, F_{px} is the projection of the cable traction force onto the x axis, T is the thrust of the engine propeller, R_x is the aerodynamic drag force UAVs and trolley, F_f is the friction force, and F_{gx} is the projection of the gravity force onto the x axis if the catapult has an elevation angle.

Let us now consider the components of Equation (7).

When solving the Equation (7), it is important to correctly take into account the change in the mass of the system M_Σ during acceleration. After the UAV takes off, Equation (7) includes only the mass m of the trolley and cable. Therefore, the moment when the UAV left the trolley was taken to be the beginning of the trolley deceleration (change of acceleration sign as a derivative of $dv/d\tau$ from positive to negative).

The traction force of the cable F_p is determined by the pressure p in the pneumatic cylinder, the area of the piston with a diameter d_p and the angle of the cable inclination β:

$$F_{px} = F_p\sin\beta = \frac{\pi}{4}d_p^2(p - p_0)\sin\beta, \quad (8)$$

where p_0 is atmospheric pressure.

The angle of the catapult elevation φ affects only the nature of the action of gravity on the trolley and the UAV (Figure 6).

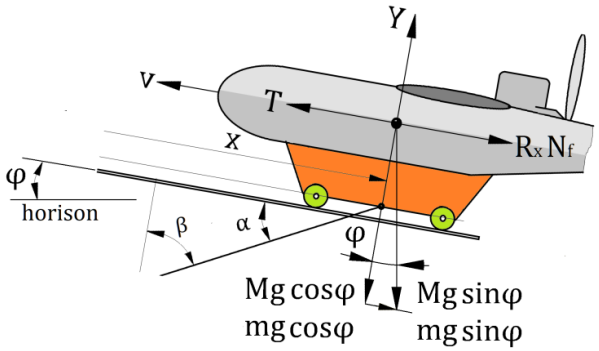

Figure 6. When the guides of the catapult are tilted, only the nature of the effect of gravity changes: in addition to reducing the normal force of pressure on the guides, an additional force of resistance to the trolley movement appears

With an increase in the angle, the force of resistance to the trolley movement from gravity increases in accordance with the Equation (9):

$$F_{gx} = g(M + m)\sin\varphi. \tag{9}$$

But the angle of the catapult does affect neither the lift force of the wing, as erroneously stated in [11], nor the aerodynamic drag of the UAV, nor the thrust of the engine propeller. However, the angle of inclination affects the friction force, since with an increase in the angle φ, the normal projection of the gravity force on the guides decreases.

In the perpendicular projection, the lifting force of the UAV wing and the corresponding projection of the cable pull force also act:

$$F_y = F_{py} + F_{gy} - Y = \frac{\pi}{4}d_p^2(p - p_0)\cos\beta + mg\cos\varphi + C\,, \tag{10}$$

where: $C = Mg\cos\beta - C_y\frac{\rho_0 v^2}{2}S$ is the pressure force of the UAV on the trolley (negative value of C means the UAV is taking off from the trolley, for this case it is necessary to take $C = 0$), F_{py} is the vertical component of the force cable pull, Y is UAV lifting force, S is wing area, and C_y is UAV aerodynamic lift coefficient.

For modeling, it is advisable to choose the parameters of specific UAVs. For example, such data for a vehicle weighing 50 kg is given in [17], including the coefficient C_y in take-off mode (equal to 0.865), as well as the wing area S=3,8 м^2.

Knowing the force F_y, it is possible to determine the rolling friction force of the trolley rollers [18]:

$$F_f = k_f F_y\,, \tag{11}$$

where k_f is the coefficient of rolling friction of the trolley rollers along the guides (according to [19], we can take $k_f = 0{,}02 - 0{,}05$).

To the friction force of the trolley rollers, it is necessary to add the friction force in the pulley bearing, which is determined by the load from the cable. In order not to complicate the task, in the 1st approximation, it was assumed that the friction force is directly proportional to the cable tension from the pneumatic cylinder piston, i.e.:

$$F_{fp} = k_{fp}(p - p_0)\frac{\pi}{4}d_p^2, \tag{12}$$

where k_{fp} is the friction coefficient of the pulley bearing (according to [18], $k_{fp} = 0{,}002$).

The UAV aerodynamic drag force is calculated by the formula:

$$R_x = C_x\frac{\rho_0 v^2}{2}S. \tag{13}$$

In take-off mode at low speeds, the aerodynamic quality of the aircraft $K = C_y/C_x$ is usually small and lies in the range of K = 3-5. The quality value was equal to 3.0, then it was used to calculate the resistance force using Equation (13). The force of the aerodynamic drag of the trolley was not taken into account in the simulation, because it is much less than UAV's, and the trolley design is unknown.

Of all the forces included in Equation (7), it remains to determine the thrust force of the propeller. According to [20, 21], the thrust T and power N of the propeller are usually represented as:

$$T = C_T \rho_0 f^2 D^4, \quad (14)$$
$$N = C_N \rho_0 f^3 D^5, \quad (15)$$

where C_T, C_N are propeller thrust and power coefficients, $f = n/60$ is rotational speed (s^{-1}), D is propeller diameter.

The thrust coefficient depends mainly on the propeller advance (slip) coefficient:

$$J = \frac{60v}{nD}. \quad (16)$$

As shown in [22], with an increase in slip, the constant pitch propeller thrust coefficient drops from approximately 0.1 to zero, and at the maximum speed of the UAV (for the selected vehicle v_{max} = 215 km/h [17]), the thrust is equal to the drag force. Then from this you can get the 2nd point on the graph $C_T = f(v)$:

$$C_T \rho_0 \left(\frac{n}{60}\right)^2 D^4 = C_y \frac{\rho_0 {v_{max}}^2}{2} S,$$

whence

$$C_{T_{vmax}} = C_y \frac{{v_{max}}^2}{2\left(\frac{n}{60}\right)^2 D^4} S. \quad (17)$$

To simulate the launch of the UAV, it is necessary to know the engine and the propeller parameters. However, at the design stage of the launcher, this data may not be known. Then the following simple algorithm can be used. From the Equation (14), it is possible to approximately find the diameter of the propeller if, using the coefficient k_T, we take into account the approximate relationship between the takeoff thrust and the takeoff weight of the UAV (preliminarily assumed k_T =0,2):

$$D = \sqrt[4]{\frac{k_T Mg}{C_T \rho_0 \left(\frac{n}{60}\right)^2}}. \quad (18)$$

The propeller diameter calculated using this formula gives quite realistic values of 0.45-0.8 m for a UAV mass in the range of 50-250 kg.

On the other hand, the Equations (14) and (15) imply:

$$\frac{N}{T} = \frac{C_n}{C_T} \frac{n}{60} D. \quad (19)$$

Using the data [22, 23] on the value of the power factor (in the 1st approximation, C_n = 0,045 is taken), from Equation (19) and the condition of equality of thrust and aerodynamic drag at the moment of UAV takeoff (at v_t =17-20 m/s), we can approximately find the engine power (in kW):

$$N = \frac{1}{120} \frac{C_y}{K} \frac{C_n}{C_T} \rho_0 {v_t}^2 DS. \quad (20)$$

Then, assuming in the 1st approximation the engine power and rotation speed are unchanged, it is possible to obtain the value of the propeller thrust in place:

$$T_0 = 60 \frac{C_n}{C_T} \frac{N}{nD}.$$

Next, approximating the dependence of C_T on v [22] with a straight line, we obtain an approximate relationship between the constant pitch propeller thrust and the flight speed:

$$T = 60 \frac{C_n}{C_T} \frac{N}{nD} \left(1 - 75 \frac{v}{nD}\right). \quad (21)$$

Dependence to Equation (21) makes it possible to approximately take into account the influence of the characteristics of the engine and propeller on the process of acceleration of the catapult trolley. Then, to solve the Equation (7), it remains only to reveal the dependence of the air pressure in the pneumatic cylinder on time.

3.1.3. Gas dynamics of pneumatic cylinder

Consider the diagram of the power part of the pneumatic system (Figure 5) – this is a cylinder with a piston, a receiver and a connecting channel with a control electro-pneumatic valve. It is assumed that the electro-valve connects the receiver with the cylinder immediately before starting, then the start is made by releasing the electric locks of the trolley.

If we neglect the hydraulic resistance of the connecting channel, then we can consider the system as a single volume. It has the equation of state for an ideal gas:

$$p = \frac{m}{V}RT\,, \tag{22}$$

where *p, T, m* are pressure, temperature and mass of air, *R* is the gas constant of air (*R* = 287.3 J/kg·K), *V* is the volume of the system, including the receiver itself V_p, the connecting channel with the front part (the cap) of the cylinder $V_0 = l_0 f_p$ and the volume $V_c = f_p x_p$, released when the piston moves in the cylinder.

That is, the volume of the system under consideration is equal to:

$$V = V_p + V_0 + V_c(x_p) = V_p + (l_0 + x_p)f_p\,, \tag{23}$$

where $f_p = (\pi/4){d_p}^2$ is the area of the cylinder with diameter d_p, l_0 is the length of the connecting channel and part of the cylinder from the end to the initial position of the piston, x_p is the current coordinate of the piston from the initial position in the cylinder (Figure 5).

After differentiation and division by *p*, the Equation (22) takes the form:

$$\frac{dp}{p} = \frac{dT}{T} + \frac{dm}{m} - \frac{dV}{V}. \tag{24}$$

On the other hand, from the energy equation, for the volume of the system [24]

$$dU = dQ - dL + idm, \tag{25}$$

where $dU = C_V d(mT)$ is the change in the internal energy of air, $dL = pdV$ is the work of air, $i = C_p T$ is the specific enthalpy, k, C_V, C_p are the adiabatic index, heat capacity at constant pressure and volume, related by the formula

$$C_p = kC_V = \frac{k}{k-1}R\,. \tag{26}$$

Let us transform the Equation (25) taking into account the fact that heat losses in the absence of heating in a fast-flowing process can be neglected:

$$mC_V dT + C_V T dm = -pdV + C_p T dm\,,$$

whence, taking into account Equation (26):

$$\frac{dT}{T} + \frac{dm}{m} = -\frac{p}{mC_V T}dV + \frac{C_p}{C_V}\frac{dm}{m}\,,$$

which allows us to obtain an equation for temperature change:

$$\frac{dT}{T} = -(k-1)\left(\frac{dm}{m} - \frac{dV}{V}\right), \tag{27}$$

and after substituting Equation (27) into Equation (24), the equation for pressure change is:

$$\frac{dp}{p} = -k\left(\frac{dm}{m} - \frac{dV}{V}\right). \tag{28}$$

If we take into account that $dV = f_p dx_p$, and $dx_p/d\tau = v_p$, then Equations (27) and (28) can be reduced to the system:

$$\begin{cases} \frac{dT}{d\tau} = (k-1)\Phi T \\ \frac{dp}{d\tau} = k\Phi p \end{cases}, \tag{29}$$

where

$$\Phi = -\frac{1}{\frac{V_p}{f_p} + l_0 + x_p}\left(v_p + \frac{RT}{pf_p}\frac{dm}{d\tau}\right).$$

Analysis of the system in Equation (29) shows that the change in temperature and pressure occurs due to expansion-compression when the piston moves in the cylinder ($v_p \neq 0$) and air leaking from the system ($dm/d\tau > 0$).

Leaks occur through the gaps between the piston and cylinder and between the cable and the cylinder head. Since the pressure drop between the cylinder and the environment is always supercritical, the instantaneous air flow can be calculated using the formula [24]

$$\frac{dm}{d\tau} = \mu f_p p \left(\frac{2}{k+1}\right)^{\frac{1}{k-1}} \sqrt{\frac{2k}{(k+1)RT}}. \quad (30)$$

In the Equation (30), the flow coefficient can be determined from the data from [25]:

$$\mu = \frac{1}{\sqrt{1+\xi_1+\xi_2+\xi_f}}, \quad (31)$$

where the coefficients of air resistance: ξ_1 – in the gap, ξ_2 – in the labyrinth (if any), ξ_f – friction, are found by the formulas:

$$\begin{cases} \xi_1 = 1 + \xi' \\ \xi_2 = n(a_0 + \xi' b_0), \\ \xi_f = \lambda l_f / d_g \end{cases} \quad (32)$$

In Equation (32) ξ'=0,5, n is the number of labyrinths on the piston, l_f is the length of the side surface of the piston/cylinder cap, $d_g = 2\sqrt{d_p \delta}$ is the characteristic size of the flow section (hydraulic diameter), δ is the radial gap. Graphs of the coefficients a_0 and b_0 [25] are approximated to formulas:

$$\begin{cases} a_0 = 0{,}87(1 - e^{-0{,}047\bar{s}}) \\ b_0 = 0{,}60(1 - e^{-0{,}0347\bar{s}}) \end{cases},$$

where $\bar{s} = s/\delta$ is the relative (to the gap) width of the labyrinth groove.

In addition, to calculate the friction coefficient ξ_f the following is calculated:

$$\lambda = (1{,}8 lg Re - 1{,}64)^{-2},$$

where $Re = \rho u d_g / \mu_0$ is the Reynolds number, μ_0 is the dynamic viscosity of the air, and the air velocity is:

$$u = \frac{RT}{\mu f_p p} \frac{dm}{d\tau}.$$

3.2. Method for solving differential equations of trolley and UAV motion

Thus, the state of air and the movement of the catapult trolley are described by a system of 4 differential equations of the 1st order, resolved with respect to the derivative:

$$\begin{cases} \frac{dv}{d\tau} = \frac{F_{px} + T - R_x - F_f - F_{gx}}{M_\Sigma} \\ \frac{dp}{d\tau} = k\Phi p, \quad \frac{dx}{d\tau} = v \\ \frac{dT}{d\tau} = (k-1)\Phi T \end{cases}, \quad (33)$$

It is expedient to solve the system in Equation (33) by a numerical method with initial conditions:

$$\tau = 0,\ v = 0,\ p = p_p,\ T = 293\text{K},\ x = L,\ x_p = l_0.$$

Due to the fact that significant gradients of parameters are possible, the improved Euler method of the 2nd order [26] was chosen to solve the equations, averaging the derivatives of the parameters at the current and previous steps:

$$f_i = f_{i-1} + \left(\frac{df_i}{d\tau} + \frac{df_{i-1}}{d\tau}\right)\frac{\Delta\tau}{2}.$$

The simulation was carried out with the following initial data: the mass of the bogie m = 10 kg, the length of the upper part of the guides L_0 = 4,5 м, the diameter of the pneumatic cylinder d_p = 75 mm and the pulley d = 150 mm at the height H=0,3 m, the volume of the receiver V_p = 40 л. The time integration step was taken 0,01 s.

4. Results

Figure 6 shows the results of modeling the speed of the trolley and the piston at the extreme values of the UAV mass (50 and 250 kg) with the correction of the pressure in the receiver to achieve the specified launch speed (17-18 m/s). Attention is drawn quickly, within about 0,55 s, to the dampened vibrations of the trolley after the UAV take-off, which is fully consistent with the properties of known launchers. It is characteristic that with increasing pressure, the frequency of natural oscillations of the catapult moving system increases (Figure 6a and 6b).

The trolley acceleration, as expected, reaches significant values precisely in the braking area after the UAV take-off (Figure 7a). The piston acceleration (Figure 7b) is many times greater, since the piston, unlike the trolley, not only slows down, but also changes the direction of movement to the opposite.

The model also makes it possible to calculate the length of the automatic braking path of the trolley after the UAV take-off (Figure 8) – the braking path is very short and does not exceed 0.5 m. No special braking devices or dampers are required for this.

Figure 9 shows the effect of air leaks from the cylinder on the pressure in it. From the nature of the pressure change (Figure 9a), it follows that leaks reduce the parameters of the launch system, but they can probably be compensated by an increase in the initial pressure in the receiver (Figure 9b).

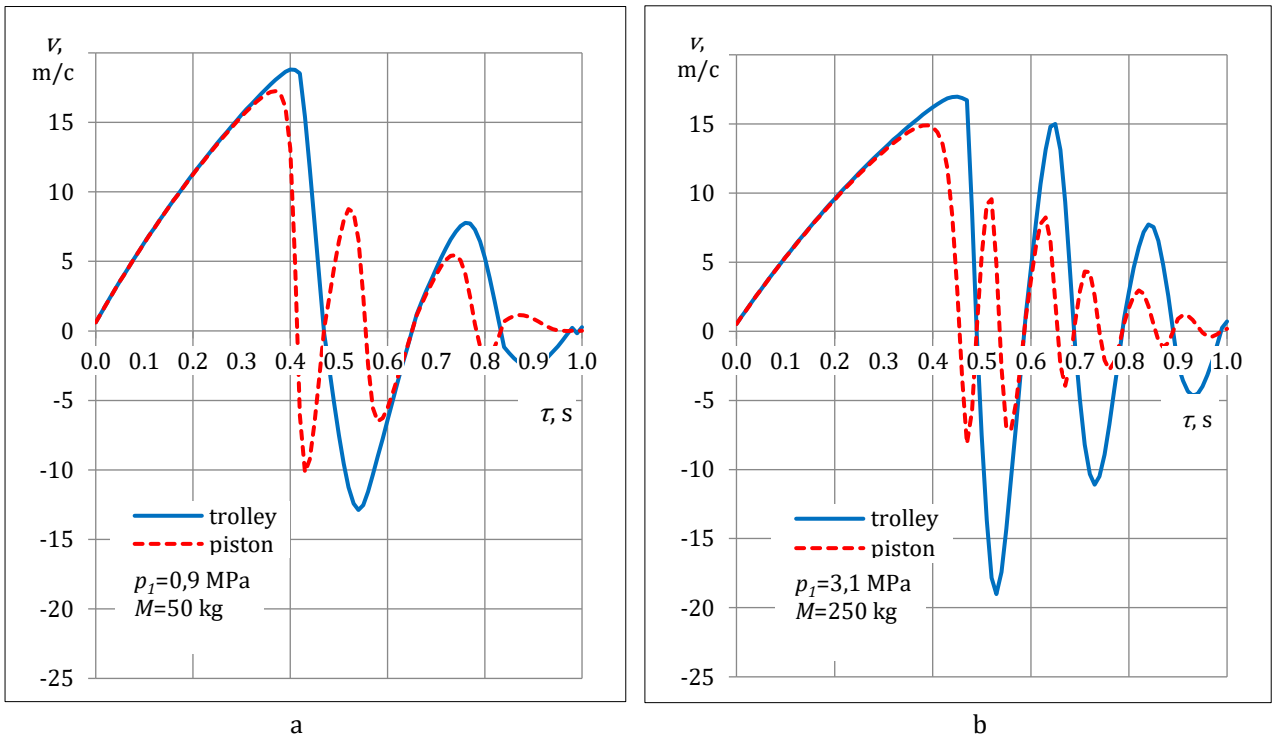

a b

Figure 6. Dependence of the trolley and piston speed on time with UAV mass of 50 kg (a) and 250 kg (b)

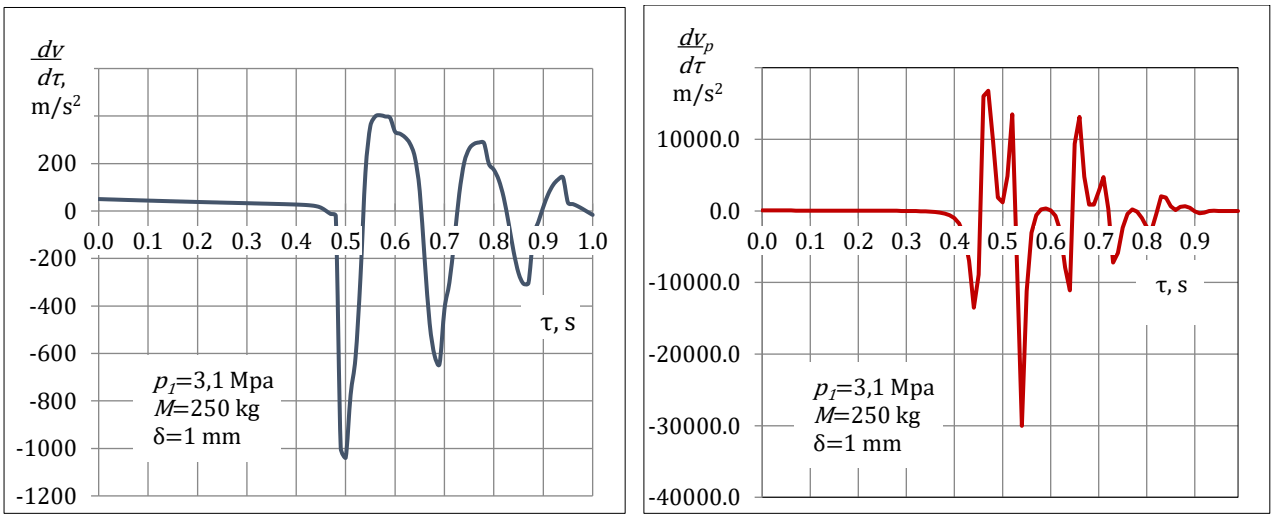

a b

Figure 7. The trolley (a) and the piston (b) acceleration during launch

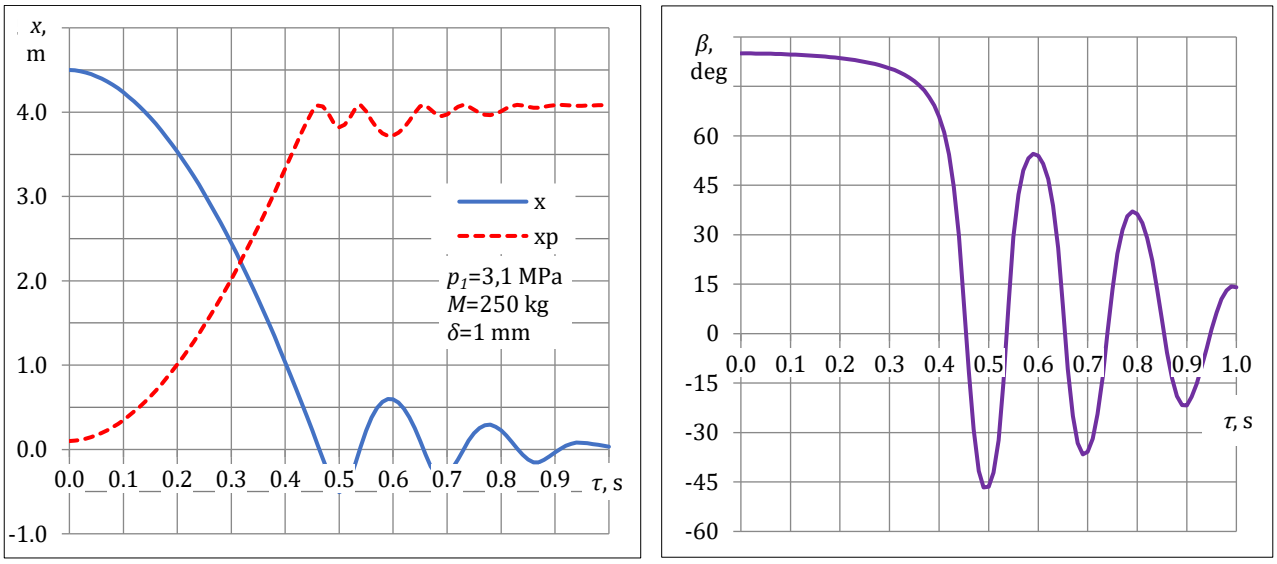

a b

Figure 8. Motion of the trolley and piston (a) versus a time; same with the angle of the cable to the vertical (b)

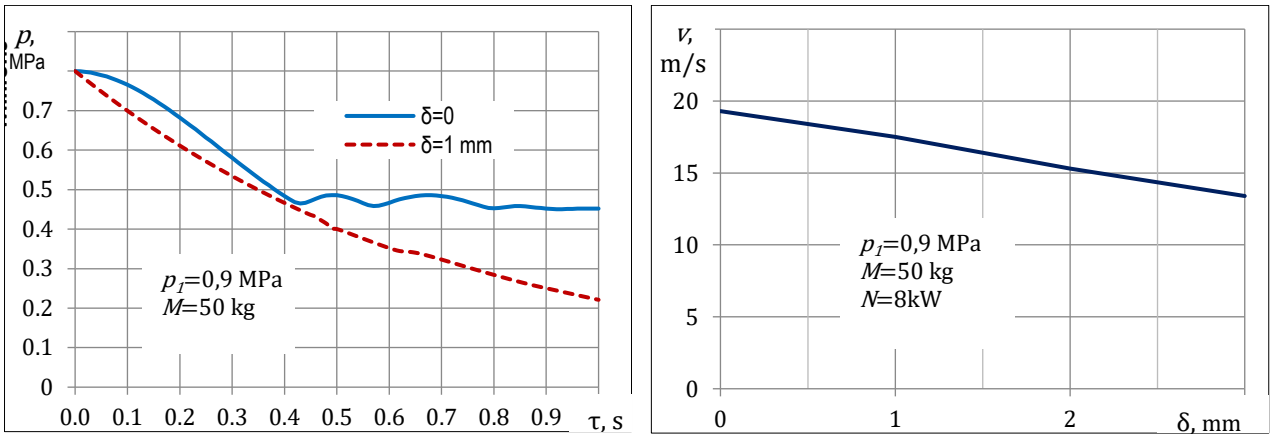

a b

Figure 9. Effect of air leakage from the cylinder on the air pressure (a) and the launch speed at the given initial pressure (b)

The power of the angle of the catapult inclination on the trolley speed at the moment of UAV lift-off is shown in Figure 10. To maintain a constant speed, it is also required to increase the pressure in the receiver by approximately 2-3% for every 10^0 lift.

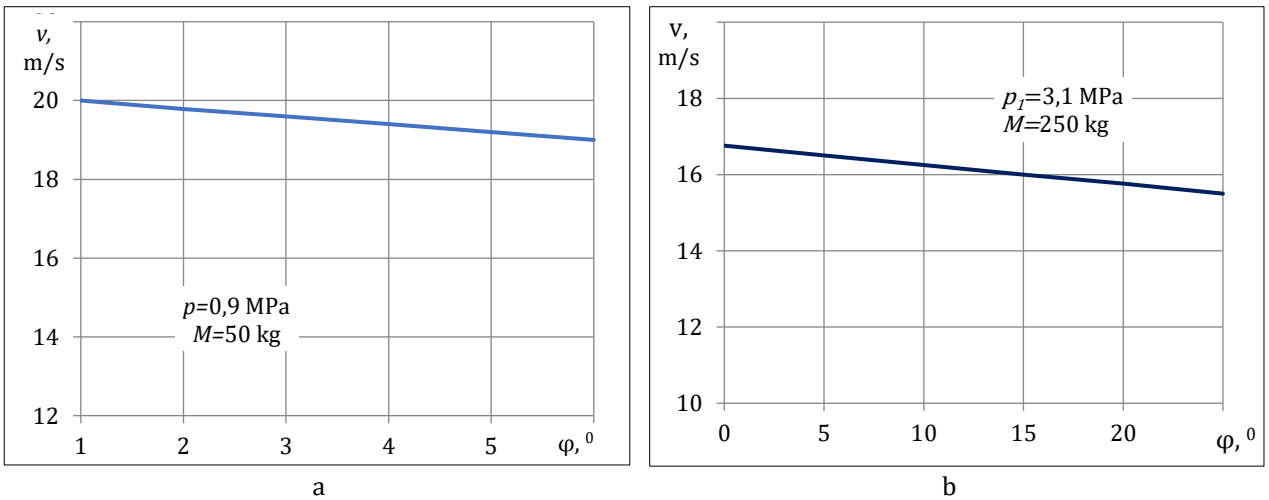

a b

Figure 10. The angle of inclination versus the launch speed at the given initial pressure

The propeller thrust is provided by the engine power and significantly increases the UAV launch speed (Figure 11a) due to the thrust contribution to the trolley acceleration (7). However, the influence of various factors, including those that worsen the parameters of the launch system, can be compensated by changing the initial pressure in the receiver (Figure 11b).

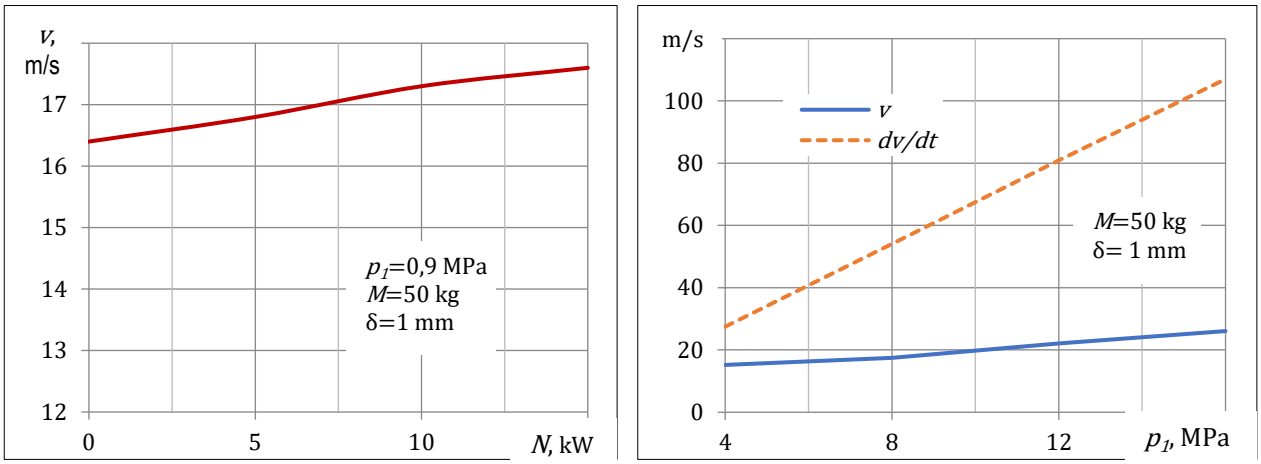

a b

Figure 11. Effect of engine power (a) and pressure in the receiver (b) on the launch speed and acceleration of the UAV

Figure 12a shows the effect of the receiver volume on the UAV launch speed, and Figure 12b shows the maximum piston accelerations in the braking mode versus the height H of the cable mount point on the trolley over the pulley axis.

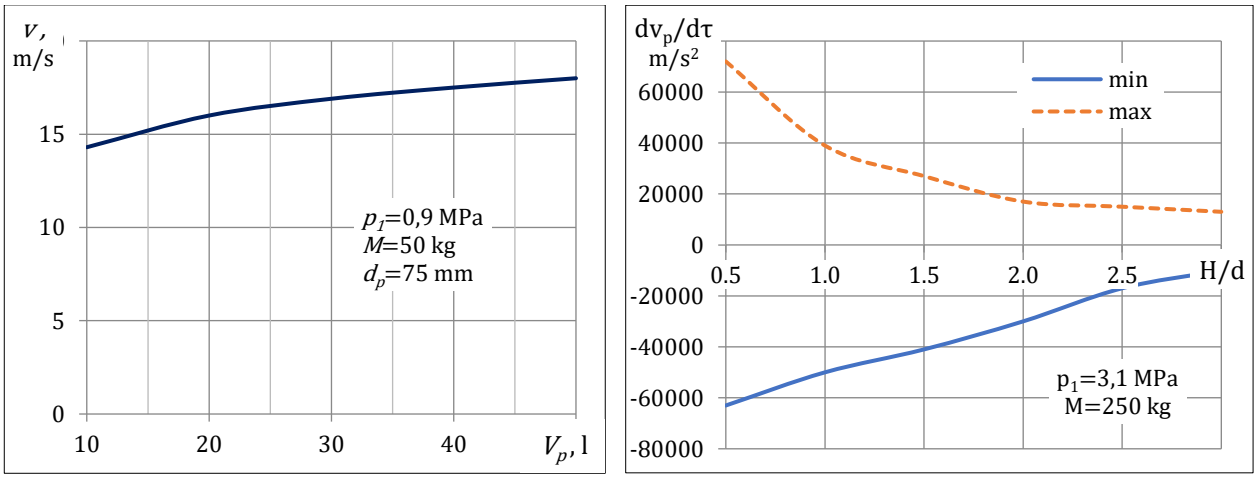

a b

Figure 12. The action of the design parameters of the catapult – the receiver volume (a) and the relative (to the diameter of the pulley) height of the cable mount point on the trolley over the pulley axis (b), on the UAV launch speed (a) and the acceleration of the pneumatic cylinder piston (b)

5. Discussion

Significant piston acceleration (Figure 7b) at high pressures in the cylinder, determined by the UAV mass, can impose restrictions on the catapult design due to the strength of the cable and pulley. Based on the acceleration values, it cannot be ruled out that the piston should be made of light but strong materials. However, this issue requires further research.

According to the simulation results (Figure 9), the seals for the piston and the cable are needed only at the initial position in the mode of launch waiting (release of the trolley locks), which is easily implemented in the design of the pneumatic cylinder. Due to the short process time, for the rest of the length of the pneumatic cylinder, the piston clearance must be selected from the condition of maximum durability of the cylinder-piston pair under real operating conditions, and not the best sealing of the high-pressure cavity of the cylinder. At the same time, leaks remain controlled even with large gaps between the piston and the cylinder. At the same time, the study shows (Figure 9) that the neglect of leaks, which is usually allowed by default in the study of pneumatic catapults, determines a significant error in the calculations.

It also follows from the obtained results (Figure 12) that the volume of the receiver, less than 30 liters, significantly reduces the parameters of the launcher, while an increase in the receiver over 40 liters has practically no effect on its operation. But at the same time, the increased receiver significantly increases the preparation time for the launcher. Based on this, the receiver volume of 30-40 l is the optimal one. With such receiver volumes, special expensive compressor equipment and significant electrical capacities can be avoided, since it becomes advisable to use portable high-pressure compressors with a capacity of 100-150 l min with an electrical power of 2-2.5 kW.

In addition, as follows from Figure 12, the decreased height of the structure (from the axis of the pulley to the point of attachment of the cable on the trolley) is less than 2-2.5 times the diameter of the pulley can lead to problems with the strength of the cable and/or piston due to a sharp increase in accelerations in trolley braking mode.

In general, any deviations in the parameters of the pneumatic launcher including the angle of the catapult elevation (Figure 10) can be compensated by changing the initial pressure in the receiver in one direction or another. However, the pressure correction (Figure 11) may have upward limits both in terms of the strength and safety of the structure itself and its elements, and in terms of the permissible acceleration of the UAV. But in any case, the determination of these limits is a topic for further study.

Thus, the developed model makes it possible to quantifiably evaluate the influence of important design parameters of the launcher on its effectiveness, which cannot be done speculatively or only with the help of simple calculation methods common in practice.

6. Conclusion

Based on the results of the study, it was found that simple methods at the level of analysis of acting forces used to evaluate the characteristics of UAV launchers do not make it possible to correctly select the type and parameters of the catapult for specific tasks. In the absence of the necessary methods, this leads to design errors that significantly narrow the scope of the launcher.

To eliminate these problems, a mathematical model of a pneumatic catapult has been developed, differential equations of motion and changes in the gas-dynamic parameters of structural elements have been compiled and numerically solved. By modeling, an analysis of the characteristics was carried out, the choice of a design scheme and the main parameters of a pneumatic catapult was substantiated.

As a result of the study, it was shown that for the effective functioning of the launcher, no special sealing of the pneumatic cylinder piston is required, and air leakage through the gap up to 1 mm is controlled due to the short process time even at high operating pressure. In addition, the permissible minimum height of the cable attachment point on the trolley above the pulley was determined, which is 2-2.5 pulley diameters, below which the loads on the cable and piston sharply increase.

Modeling the UAV launch processes using the developed model confirmed the versatility of using a pneumatic catapult of the selected type for operational-tactical UAVs with a take-off weight of 50 to 250 kg. Such a wide range is provided only by regulating the air pressure in the receiver within 0.5-3.0 MPa and is not available in launch systems of other types, and the filling of the receiver for the next start is quickly achieved using inexpensive portable high-pressure compressors. At the same time, if the increase in pressure above 3.0 MPa can be limited by safety requirements, the possibility of increasing the UAV take-off weight above 250 kg is preserved by increasing the diameter of the pneumatic cylinder. These advantages of pneumatic launch systems indicate that further research should be directed to the development of individual elements of the launch system design in order to cover an even wider range of UAVs.

Acknowledgement

Gratitude to Machining Center «AB-Engineering», Odessa, and International Motor Bureau, Nemishayeve, Kyiv region, Ukraine, for technical support and provision of the materials for research.

Funding

This research received no external funding.

Conflicts of interest

The author declares no conflicts of interest.

References

1. Cearns, J., Huxley, S., Garcia, D., & Lacasse, B. (2019). UAV catapult. California Polytechnic State University, 140.
2. Novaković, Z., Vasić, Z., Ilić, I., Medar, N., & Stevanović, C. (2016). Integration of тactical-medium range UAV and catapult launch system. Scientific Technical Review, 66(4), 22-28.
3. Barnhart, R. K., Hottman, S. B., Marshall, D. M., & Shappee, E. (2012). Introduction to unmanned aircraft systems. CRC Press
4. Austin, R. (2010). Unmanned aircraft systems: UAVs design, development and deployment. John Wiley & Sons
5. Kondratiuk, M., & Ambroziak, L. (2020). Design and dynamics of kinetic launcher for unmanned aerial vehicles. Applied Science, 10(8), 2949. https://doi.org/10.3390/app10082949.
6. Bumb N., Kalogeropoulos, X., Kelday, A., Wai Hou, L., Xiao, L., Portakalcioglu, H., Tagg, J., Tarazi, B. (2012). Catapult launcher for Unmanned Air Vehicles (UAV). Part 2. Design case study. SESM2005: Engineering Design and Structural Analysis Methods. 86. https://dokumen.tips/documents/catapult-launcher-for-uav.html?page=3
7. Jastrzębski, G. (2016). Impact of opening time of the take-off pneumatic launcher main valve on take-off pressure losses. Journal of KONES Powertrain and Transport, 23(4), 175-182.
8. Ukrspecsystems Ukraine Releases (2020). New UAV Bungee Catapult Launcher. UAS Weekly, 2. https://uasweekly.com/2020/11/22/ukrspecsystems-releases-new-uav-bungee-catapult-launcher/
9. Novaković Z., Medar, N., & Mitrović, L. (2014). Increasing launch capability of a UAV bungee catapult. Scientific Technical Review, 64(4), 17-26.
10. Miller, B., Valoria, Ch., Warnock, C., & Coutlee, J. (2014). Lightweight UAV. Launcher senior project for Aerojet-Rocketdyne. Final Report. California Polytechnic State University, Saint Luis. 232.
11. Jurczyk, K. (2018). The prospect for the launche of a mini unmanned aerial vehicle from an unmanned surface vehicle. Scientific Journal of Polish Naval Academy, 1(212), 5-26. https://doi.org/10.2478/sjpna-2018-0001.
12. Pneumatic UAV launcher GLS-1A. (2023). Ukrspecsystems Ukraine. AeroExpo, 1. https://www. aeroexpo.online/prod/ukrspecsystems/ product-185884-73131.html
13. Gan, L., Fang, X., Zhang, Zh., Chen, H., Wei, X. (2022). Modular clustering of uav launch system architecture based on HDDSM. Aerospace, 9 (168), 18. https://doi.org/10.3390/ aerospace9030168.
14. Grekov, V. P., & Tkachenko, Yu. A. (2018). Calculation of a single-stage pneumatic cylinder with a built-in receiver as a ground-based drive. Weapon systems and military equipment, 1(53), 91-96. https://doi.org/10.30748/ soivt.2018.53.13. (In Ukrainian).
15. To the commander of the unit for the use of tactical-level UAC (based on the experience of carrying out OOS (formerly ATO) (2022). Center for educational literature, Kyiv, 66. (In Ukrainian).
16. Theory and practice of using unmanned aerial vehicles (drones). (2023). LITERA, Kyiv, 126. (In Ukrainian).
17. Lemko, O. L., & Molodchik, A. D. (2015). Aerodynamic and flight technical characteristics of the promising unmanned aerial vehicle of the "flying wing" scheme. Mechanics of gyroscopic systems, 29, 44-52. http://dx.doi.org/10.20535/0203-3771292015671 72. (In Ukrainian).
18. Lippert, D., & Spektor, J. (2013). Rolling resistance and industrial wheels. *Hamilton White Paper*, (11).
19. NSK Rolling Bearings. (2013). Cat. No. E1102m. NSK Ltd., Tokio, 283.
20. Podsędkowski, M., Konopiński, R., Obidowski, D., & Koter, K. (2020). Variable pitch propeller for UAV-experimental tests. *Energies*, *13*(20), 5264. http://dx.doi.org/10.3390/en13205264.
21. Stokkermans, T. C. A. (2020). Aerodynamics of propellers in interaction dominated flowfields: An application to novel aerospace vehicles. Doctoral Dissertation, Delft University of Technology
22. Brandt, J. B., Deters, R. W., Ananda, G. K., Dantsker, O. D., & Selig, M. S. (2020). UIUC Propeller Data Site. Department of Aerospace Engineering. https://m-selig.ae.illinois.edu/props/ propDB.html
23. Gill, R., & D'Andrea, R. (2019). Computationally efficient force and moment models for propellers in UAV forward flight applications. Drones, 3(77), 47. http://dx.doi.org/10.3390/drones3040077.
24. Ercan, A. (2021). Analysis and design of a novel reciprocating compressor utilizing a minfas-tar mechanism. Doctoral Dissertation, Middle East Technical University.
25. Idel'chik, E. (1966). Handbook of hydraulic resistance. Coefficients of local resistance and of frictio. Israel Program for Scientific Translations Ltd., Springfield, 517.
26. Zadachin, V. M., & Koniushenko, I. G. (2014). Numerical methods: tutorial. Pub. KhNEU im. S. Kuznetsa, Kharkiv, 180. (In Ukrainian).